# An efficient and robust monolithic approach to phase-field quasi-static brittle fracture using a modified Newton method

Olivier Lampron[a], Daniel Therriault[a], Martin Lévesque[a,*]

[a]*Laboratory for Multiscale Mechanics, Department of Mechanical Engineering, Polytechnique Montreal, 2900 boul. Edouard-Montpetit, Montreal, QC, Canada*

**Abstract**

Variational phase-field methods have been shown powerful for the modeling of complex crack propagation without a priori knowledge of the crack path or ad hoc criteria. However, phase-field models suffer from their energy functional being non-linear and non-convex, while requiring a very fine mesh to capture the damage gradient. This implies a high computational cost, limiting concrete engineering applications of the method. In this work, we propose an efficient and robust fully monolithic solver for phase-field fracture using a modified Newton method with inertia correction and an energy line-search. To illustrate the gains in efficiency obtained with our approach, we compare it to two popular methods for phase-field fracture, namely the alternating minimization and the quasi-monolithic schemes. To facilitate the evaluation of the quasi-monolithic scheme, we couple the latter with an extrapolation correction loop controlled by a damage-based criteria. Finally, we show through four benchmark tests that the modified Newton method we propose is straightforward, robust and leads to identical solutions, while offering a reduction in computation time by factors of up to 12 and 6 when compared to the alternating minimization and quasi-monolithic schemes.

*Keywords:* Phase-field, variational, fracture, quasi-static, implicit, monolithic, quasi-monolithic, staggered, benchmark

## 1. Introduction

The variational reformulation of Griffith's theory [1] proposed by Francfort and Marigo [2] and followed by Bourdin et al.'s numerical treatment [3] offered a robust mathematical and computational framework for the modeling of quasi-static brittle fracture. Based on a smooth representation of the discontinuities through a damage field, variational phase-field models compute the nucleation and propagation of complex crack paths through the minimization of an energy functional. As opposed to discrete approaches dealing explicitly with cracks like the Linear Elastic Fracture Mechanics (LEFM) or the Cohezive Zone Model technique (CZM), the phase-field method for fracture can model crack propagation without the need for remeshing, a priori knowledge of the crack path or any ad hoc criteria [4]. Owing to its elegant simplicity and its compatibility with classical finite element methods, the phase-field method has been applied and extended to hydraulic fracture [5, 6], ductile fracture [7, 8], stress corrosion cracking [9, 10] and brittle fracture in heterogeneous structures [11, 12].

A well-known downside of the phase-field method is its high computational cost. The first explanation for this is the necessity of a very fine mesh for the finite element method to accurately capture the strong damage gradient in the fracture zone, yielding large linear systems to be solved. Adaptive mesh techniques [13, 14, 15] and multiscale methods [16, 17] have been developed and appear to successfully reduce the number of degrees of freedom to a minimum.

*Corresponding author
*Email address:* martin.levesque@polymtl.ca (Martin Lévesque)

The second explanation for the high computational cost is the non-linear and non-convex nature of the underlying energy functional of phase-field models [3]. For non-convex problems, the conventional Newton's method is inadequate since the Hessian can become indefinite and hinder the convergence to a critical point. The first method proposed in the literature to solve phase-field models was the alternating minimization algorithm [3]. Stemming from the observation that the functional is convex in each variable when the other field is fixed, the alternating minimization scheme alternatively solves the kinematic and damage sub-problems until convergence. Widely adopted by the community [10, 11, 18, 19, 20, 21, 22, 23, 24, 25], the algorithm is robust, but exhibits an infamously slow convergence rate due to the decoupling of the sub-problems [26, 27, 28]. Significant gains in efficiency were obtained using a combination of preconditioned alternative minimization scheme and classical Newton's method [27], or a semi-implicit form of the staggered scheme [29]. Nevertheless, such methods require either the tuning of a numerical parameter or a time step convergence study, implying additional computation, while still suffering from the decoupling between the displacement and damage fields.

The quasi-monolithic approach was proposed [13] to deal with a convex problem while retaining the coupling between the fields. This *convexification* of the functional through a time extrapolation of the phase-field was used in [30, 31, 32]. The quasi-monolithic scheme was also reported efficient and robust, but the relaxation of the applied forces and a delayed crack growth was observed [33]. Furthermore, the delayed and relaxed evolution seems to be amplified under unstable crack growth, where the damage field evolves rapidly. This suggests that the quasi-monolithic scheme generates a numerical viscosity, requiring smaller time steps and, therefore, an increased computational cost to accurately capture rapidly growing cracks. To the best of our knowledge, the efficiency of the alternating minimization algorithm and the quasi-monolithic scheme has never been compared.

A fully monolithic scheme would have the potential to be more efficient and accurate than the alternating and quasi-monolithic methods since it would preserve the strong coupling between the two fields. As reported by Wick [34], obtaining a monolithic scheme for phase-field models for fracture is a difficult task. Numerous monolithic algorithms have been proposed, such as a Newton method using a modified line search algorithm [26], an error-oriented Newton's method [33], and a modified Newton method with Jacobian modification [34]. Probably due to their complexity, variable robustness or problem-dependent efficiency, these monolithic methods have yet to impose themselves, with the alternating minimization algorithm and quasi-monolithic scheme still being vastly more represented in the literature. The need for an efficient and robust solver remains to this day.

We also point out that few popular formulations such as the history variable approach of Miehe [35] or the hybrid model from [36], although computationally efficient, have the downfall of being variationally inconsistent. Gerasimov and De Lorenzis recently came to the conclusion that the approach based on the history variable proposed by Miehe [35] leads to the solution of a problem that is not equivalent to the variational one [25]. Therefore, we focus in this work on the efficiency of solvers for variational phase-field models.

In this work, we propose a fully monolithic solver relying on a modified Newton method with inertia correction of the Jacobian and a backtracking energy line-search. The modified Newton scheme is inspired by the one implemented in the well-known optimization software IPOPT [37]. We also present a comparison of the performance of the alternating minimization algorithm, the quasi-monolithic scheme and the modified Newton solver on four benchmark tests selected from the phase-field literature. To eliminate the time step dependency of the quasi-monolithic scheme and facilitate its benchmarking, we couple the latter with an extrapolation correction loop controlled by a damage evolution criteria. The results of the benchmarking demonstrate that not only is the modified Newton method a robust monolithic solver for variational phase-field models, but it is also significantly more efficient than the quasi-monolithic and alternating minimization algorithms.

The paper is organized as follows. In Section 2, we recall the formulation of variational phase-field models, describe the adopted treatment of the irreversibility constraint and write the Euler-Lagrange equations of the minimization problem along with their discretization. We also present the widely used alternating minimization algorithm, followed by the more recently studied quasi-monolithic scheme. In Section 3, we propose a monolithic solver for variational phase-field models based on a modified Newton method and

describe the quasi-monolithic scheme augmented with an extrapolation correction loop. Section 4 compares the performance of the three studied algorithms on four different benchmark tests and discusses the results. Finally, our conclusions are presented in Section 5.

## 2. Background

### *2.1. Variational modeling of brittle fracture*

Here we define the phase-field model for brittle fracture, including the strain energy decomposition and treatment of the irreversibility condition adopted, on which will be performed the benchmarking of the three solvers. Then, the Euler-Lagrange equations of the unconstrained variational problem and their spatial discretization are defined.

#### *2.1.1. Variational formulation*

We introduce $\Omega \subset \mathbb{R}^n$ $(n = 2, 3)$, the domain representing the crack-free brittle elastic body. The boundary $\partial\Omega$ is subject to time dependant Dirichlet and Neumann conditions, $\Gamma_D \subset \partial\Omega$, $\Gamma_N \subset \partial\Omega$, with $\Gamma_D \cup \Gamma_N = \partial\Omega$ and $\Gamma_D \cap \Gamma_N = \emptyset$. We also introduce the evolving crack surface $\Gamma_c \subset \Omega$. We define the displacement function $\boldsymbol{u} : \Omega \setminus \Gamma_c \subset \mathbb{R}^n \to \mathbb{R}^n$ and the linearised elastic strain $e(\boldsymbol{u}) \coloneqq \frac{1}{2}(\nabla \boldsymbol{u}^T + \nabla \boldsymbol{u})$. We can therefore define the elastic potential energy $\Psi(\boldsymbol{u}) = \frac{1}{2}\sigma(\boldsymbol{u}) : e(\boldsymbol{u})$, where $\sigma(\boldsymbol{u})$ is the stress tensor. Finally, we denote the critical energy release rate of the brittle material with $G_c$.

Neglecting the traction forces, Francfort and Marigo's reformulation's of quasi-static brittle fracture [2] leads to the following variational problem

$$\boldsymbol{u}, \Gamma_c = \arg\min \mathcal{E}(\boldsymbol{u}, \Gamma_c) \quad \text{s.t.} \quad \dot{\Gamma}_c \geq 0, \tag{1}$$

with the energy functional

$$\mathcal{E}(\boldsymbol{u}, \Gamma_c) = \int_{\Omega \setminus \Gamma_c} \Psi(\boldsymbol{u}) \, \mathrm{d}\boldsymbol{x} + \int_{\Gamma_c} G_c \, \mathrm{d}s. \tag{2}$$

Phase-field damage models use the Ambrosio and Tortorelli elliptical regularization [38] to overcome problems associated with the numerical treatment of the discontinuous crack $\Gamma_c$, as proposed initially in [3]. The regularization replaces the sharp crack by a diffuse damage band through the phase-field variable, denoted by $d : \Omega \to [0, 1]$, where $d = 0$ describes the undamaged material and $d = 1$ describes the fully damaged material. The displacement function becomes $\boldsymbol{u} : \Omega \subset \mathbb{R}^n \to \mathbb{R}^n$. The different phase-field models for fracture are characterised mainly by the type of crack function $\alpha(d)$ and degradation function $g(d)$ adopted. They can generally be expressed as

$$\mathcal{E}_l(\boldsymbol{u}, d) = \int_\Omega g(d)\Psi(\boldsymbol{u}) \, \mathrm{d}\boldsymbol{x} + \frac{G_c}{c_\alpha} \int_\Omega \Big( \frac{\alpha(d)}{l} + l|\nabla d|^2 \Big) \mathrm{d}\boldsymbol{x}, \tag{3}$$

with the normalization parameter $c_\alpha \coloneqq 4 \int_0^1 \sqrt{\alpha(z)} \, \mathrm{d}z$ [24, 25]. The regularization $\alpha(d)$ and the characteristic length $l$ define the shape and width of the smeared crack while the degradation function $g(d)$ describes the dependency of the apparent stiffness on the damage field. In this paper, we focus on the so-called $AT_1$ model with its linear crack function $\alpha(d) = d$ and quadratic degradation function $g(d) = (1-d)^2$ introduced by Pham et al. [39], yielding the functional

$$\mathcal{E}_l(\boldsymbol{u}, d) = \int_\Omega (1-d)^2 \Psi(\boldsymbol{u}) \, \mathrm{d}\boldsymbol{x} + \frac{3G_c}{8} \int_\Omega \Big( \frac{d}{l} + l|\nabla d|^2 \Big) \mathrm{d}\boldsymbol{x}. \tag{4}$$

With the regularized energy functional relying on the phase-field variable, the variational problem now reads

$$\boldsymbol{u}, d = \arg\min \mathcal{E}_l(\boldsymbol{u}, d) \quad \text{s.t.} \quad 0 \leq d \leq 1 \quad \text{and} \quad \dot{d} \geq 0. \tag{5}$$

As opposed to the widely used $AT_2$ model, the $AT_1$ prevents damage initiation at low strain-energy densities, therefore exhibiting an elastic phase. Furthermore, the linear crack function of the $AT_1$ model

leads to a finite localization band, implying the convergence to the Griffith energy without the necessity of the characteristic length $l$ to approach zero [24]. However, the constraint $d \geq 0$ from the minimization problem (5) is no longer naturally respected.

A well-known issue with formulation (4) is its inability to distinguish between energy generated from tensile or compressive loading. Consequently, interpenetration of crack surfaces and non-physical cracks were observed early in the developments of the variational approach to fracture [3]. Multiple methods using energy splits have been proposed to elude this difficulty [40, 41, 42, 43], such as the volumetric-deviatoric split [18] adopted in [44, 45] and the spectral split [35] adopted in [23, 34]. In this work, we adopt the spectral decomposition of the strain tensor in its positive and negative components, as proposed by Miehe [35], with

$$e(\boldsymbol{u}) = e^+(\boldsymbol{u}) + e^-(\boldsymbol{u}), \tag{6}$$

and

$$e^+(\boldsymbol{u}) = S(\boldsymbol{u})\Lambda^+(\boldsymbol{u})S^T(\boldsymbol{u}), \tag{7}$$

where $\Lambda^+$ is the diagonal matrix containing the positive eigenvalues $\lambda_i$, and $S$ is the matrix containing the corresponding eigenvectors $v_i$ [33]. Dropping the dependencies in $\boldsymbol{u}$, the positive and negative stress of an isotropic material now read

$$\sigma^+ = \lambda\langle \mathrm{tr}(e)\rangle_+ I + 2\mu e^+, \tag{8}$$

$$\sigma^- = \lambda\langle \mathrm{tr}(e)\rangle_- I + 2\mu e^-, \tag{9}$$

where $I$ is the second order identity tensor and ($\lambda$, $\mu$) are the Lamé coefficients. $\langle z\rangle_\pm$ designates the positive or negative ramp function of $z$, where $\langle z\rangle_+ = \max(0, z)$ and $\langle z\rangle_- = \min(0, z)$. The energy functional using the energy split becomes

$$\mathcal{E}_l(\boldsymbol{u}, d) = \int_\Omega \frac{1}{2}\Big((1-d)^2\sigma^+(\boldsymbol{u}) + \sigma^-(\boldsymbol{u})\Big) : e(\boldsymbol{u})\,\mathrm{d}\boldsymbol{x} + \frac{3G_c}{8}\int_\Omega \Big(\frac{d}{l} + l|\nabla d|^2\Big)\mathrm{d}\boldsymbol{x}. \tag{10}$$

*2.1.2. Irreversibility constraint*

Formulation (10) is set in a quasi-static regime, with dependency on time appearing only through the boundary conditions. However, the irreversibility condition found in (5) implies a history dependency in the minimization problem. Introducing a discretization of the loading process through the pseudo-time steps $\Delta t^n = t^n - t^{n-1}$, and knowing the solution from the previous step, we look for a solution to the minimization problem at every time increment. Using the time discretization, $\dot{d} \geq 0$ can be approximated through a backward differentiation with

$$d^n \geq d^{n-1}. \tag{11}$$

To avoid a cumbersome notation, we denote the solution of the actual increment $(\boldsymbol{u}^n, d^n)$ with $(\boldsymbol{u}, d)$.

The variational problem (5) now contains 3 constraints, namely $d \geq 0$, $d \leq 1$ and $d \geq d^{n-1}$. With the degradation function chosen as quadratic, $d \leq 1$ is naturally respected [46]. However, $d \geq 0$ and $d \geq d^{n-1}$ need to be imposed. Multiple options for enforcing the $d \geq d^{n-1}$ condition are available in the literature, such as the augmented Lagrangian method [47], the penalty method [25] or the algorithm presented in [29] (see [25, 29] for a review of them). Here we adopt the simple quadratic penalty, as proposed by [25]

$$P = \frac{\gamma}{2}\int_\Omega \langle d - d^{n-1}\rangle_-^2\,\mathrm{d}\boldsymbol{x}, \tag{12}$$

where $\gamma$ is a penalty parameter and $d^{n-1}$ is the solution of the phase-field from the previous time increment. By taking $d^0 \geq 0$, the constraint $d \geq 0$ is simultaneously enforced. Adding penalty term (12) to the energy functional (10) yields an unconstrained minimization problem which reads

$$\boldsymbol{u}, d = \arg\min\, \mathcal{E}_l(\boldsymbol{u}, d) \tag{13}$$

with the energy functional

$$\mathcal{E}_l(\boldsymbol{u}, d) = \int_\Omega \frac{1}{2}\Big((1-d)^2\sigma^+(\boldsymbol{u}) + \sigma^-(\boldsymbol{u})\Big) : e(\boldsymbol{u})\,\mathrm{d}\boldsymbol{x} + \frac{3G_c}{8}\int_\Omega \Big(\frac{d}{l} + l|\nabla d|^2\Big)\mathrm{d}\boldsymbol{x} + \frac{\gamma}{2}\int_\Omega \langle d - d^{n-1}\rangle_-^2\,\mathrm{d}\boldsymbol{x}. \quad (14)$$

This new problem is an approximation of (5), where the minimizers of (14) converge to the minimizers of (10) with $\gamma \to \infty$. Instead of increasing $\gamma$ until the Karush-Kuhn-Tucker (KKT) conditions are met, as one would typically do with a penalty method, we use the fixed optimal penalty parameter presented in [25]

$$\gamma = \frac{G_c}{l}\frac{27}{64\mathtt{TOL}_{\mathtt{Ir}}^2}, \quad (15)$$

where $\mathtt{TOL}_{\mathtt{Ir}}$ is a chosen irreversibility tolerance. Derived from the notion of optimal phase-field profile, this constant penalty coefficient was shown to lead to a good approximation of the original constrained problem [25].

*2.1.3. Euler-Lagrange equations and finite element discretization*

By introducing the function spaces $\boldsymbol{\mathcal{V}} \coloneqq (H^1_{\Gamma_D}(\Omega))^n$ and $\mathcal{W} \coloneqq H^1(\Omega)$, with $H^1(\Omega)$ the Sobolev space, and applying directional derivatives towards $(\boldsymbol{u}, d)$ to (14), the Euler-Lagrange equations of problem (13) can be written in their weak form as [13, 25]: Find $\boldsymbol{u} \in \boldsymbol{\mathcal{V}}$ and $d \in \mathcal{W}$ such that

$$\int_\Omega \Big((1-d)^2\sigma^+(\boldsymbol{u}) + \sigma^-(\boldsymbol{u})\Big) : e(\boldsymbol{v})\,\mathrm{d}\boldsymbol{x} = 0, \quad \forall \boldsymbol{v} \in \boldsymbol{\mathcal{V}}, \quad (16a)$$

$$\int_\Omega -w(1-d)\sigma^+(\boldsymbol{u}) : e(\boldsymbol{u})\,\mathrm{d}\boldsymbol{x} + \frac{3G_c}{8}\int_\Omega \Big(\frac{w}{l} + 2l\nabla d\cdot\nabla w\Big)\mathrm{d}\boldsymbol{x} + \gamma\int_\Omega w\langle d - d^{n-1}\rangle_-\,\mathrm{d}\boldsymbol{x} = 0, \quad \forall w \in \mathcal{W}. \quad (16b)$$

The equation system (16) is usually discretized using a Galerkin finite element method [13, 19, 32]. To this end, assuming a 2D polygonal domain, we partition $\Omega$ in a non-degenerate family of quadrilateral elements $\mathcal{Q}^h$, where $h$ is the average element edge size. Using the notation from [48], we introduce the linear finite element space

$$\mathcal{V}_h \coloneqq \{v \in H^1(\Omega) :\ v|_Q \text{ is linear } \forall Q \in \mathcal{Q}^h\}.$$

The nodal basis functions of the vector space $\mathcal{V}_h$ are noted

$$\{\varphi_i : 1 \le i \le m\},$$

where $m$ is the dimension of the finite element space. To approximate the vector field $\boldsymbol{u}$, and borrowing the deal.II convention [49], we define the $2m$ vector shape functions

$$\boldsymbol{\phi}_0(\boldsymbol{x}) = \begin{pmatrix}\varphi_0(\boldsymbol{x})\\ 0\end{pmatrix},$$
$$\boldsymbol{\phi}_1(\boldsymbol{x}) = \begin{pmatrix}0\\ \varphi_0(\boldsymbol{x})\end{pmatrix},$$
$$\boldsymbol{\phi}_2(\boldsymbol{x}) = \begin{pmatrix}\varphi_1(\boldsymbol{x})\\ 0\end{pmatrix}\dots$$
$$\boldsymbol{\phi}_{2m}(\boldsymbol{x}) = \begin{pmatrix}0\\ \varphi_m(\boldsymbol{x})\end{pmatrix}.$$

Collecting the displacement and damage nodal coefficients in respectively $\boldsymbol{U} \in \mathbb{R}^{2m}$ and $\boldsymbol{D} \in \mathbb{R}^m$, the functions $(\boldsymbol{u}, d)$ are now approximated with

$$\boldsymbol{u}_h(\boldsymbol{x}) = \sum_{j=1}^{2m}\boldsymbol{\phi}_j(\boldsymbol{x})U_j, \quad d_h(\boldsymbol{x}) = \sum_{j=1}^{m}\varphi_j(\boldsymbol{x})D_j. \quad (17)$$

Using the finite element approximations $\boldsymbol{u}_h \in \mathcal{V}_h \times \mathcal{V}_h$ and $d_h \in \mathcal{V}_h$, the discretized Euler-Lagrange equations can be written as the following residuals

$$R_i^u \coloneqq \int_\Omega \Big((1-d_h)^2\sigma^+(\boldsymbol{u}_h) + \sigma^-(\boldsymbol{u}_h)\Big) : e(\boldsymbol{\phi}_i)\,\mathrm{d}\boldsymbol{x} = 0 \tag{18a}$$

$$R_i^d \coloneqq \int_\Omega -(1-d_h)\varphi_i\sigma^+(\boldsymbol{u}_h) : e(\boldsymbol{u}_h)\,\mathrm{d}\boldsymbol{x} + \frac{3G_c}{8}\int_\Omega \Big(\frac{\varphi_i}{l} + 2l\nabla d_h \cdot \nabla\varphi_i\Big)\mathrm{d}\boldsymbol{x} + \gamma\int_\Omega \varphi_i\langle d_h - d_h^{n-1}\rangle_-\,\mathrm{d}\boldsymbol{x} = 0. \tag{18b}$$

For all Newton-based solvers, the assembly of the Jacobian, or at least part of it, is necessary. The Jacobian associated to (18) can be written in its block structure as

$$J_{ij}^{uu} = \frac{\partial R_i^u}{\partial U_j} = \int_\Omega \Big((1-d_h)^2\sigma^+(\boldsymbol{\phi}_j) + \sigma^-(\boldsymbol{\phi}_j)\Big) : e(\boldsymbol{\phi}_i)\,\mathrm{d}\boldsymbol{x} \tag{19a}$$

$$J_{ij}^{ud} = \frac{\partial R_i^u}{\partial D_j} = \int_\Omega -2(1-d_h)\varphi_j\sigma^+(\boldsymbol{u}_h) : e(\boldsymbol{\phi}_i)\,\mathrm{d}\boldsymbol{x} \tag{19b}$$

$$J_{ij}^{du} = \frac{\partial R_i^d}{\partial U_j} = \int_\Omega -2(1-d_h)\varphi_i\sigma^+(\boldsymbol{u}_h) : e(\boldsymbol{\phi}_j)\,\mathrm{d}\boldsymbol{x} \tag{19c}$$

$$J_{ij}^{dd} = \frac{\partial R_i^d}{\partial D_j} = \int_\Omega \varphi_i\varphi_j\sigma^+(\boldsymbol{u}_h) : e(\boldsymbol{u}_h)\mathrm{d}\boldsymbol{x} + \frac{3G_c}{8}\int_\Omega 2l\nabla\varphi_i \cdot \nabla\varphi_j\mathrm{d}\boldsymbol{x} + \gamma\int_\Omega \varphi_i\varphi_j H^-(d_h - d_h^{n-1})\,\mathrm{d}\boldsymbol{x}, \tag{19d}$$

with the general structure

$$J = \begin{pmatrix} J^{uu} & J^{ud} \\ J^{du} & J^{dd} \end{pmatrix}. \tag{20}$$

By $\sigma^+(\delta\boldsymbol{u})$, we imply the directional derivative of $\sigma^+$ towards $\boldsymbol{u}$ as thoroughly detailed by [13]. Stemming from the derivative of the ramp function $\langle z\rangle_-$, $H^-(z)$ is the Heaviside function worth 1 if $z \leq 0$ and worth 0 otherwise. Finally, we denote the discretized Dirichlet conditions $\bar{\boldsymbol{U}}$.

### *2.2. Solution algorithms*

We present two algorithms commonly used to obtain a solution in phase-field fracture problems: the alternating minimization algorithm and the quasi-monolithic scheme. With these two methods, the Euler-Lagrange equations (16) are treated as a set of non-linear equations and only a stationary point of (14) is obtained. The nature of the stationary point as either a local minimum, saddle point or local maximum is unknown.

#### *2.2.1. Alternating minimization algorithm*

As observed in [3], the functional (4) becomes convex in one field when the other is fixed. A critical point can therefore be easily obtained with the Newton method if we solve towards one field at a time. Based on this fact, the alternating minimization algorithm, also often referred to as the staggered solver, consists in splitting the problem in a kinematic and a damage sub-problem and, as its name implies, alternatively solving them until global convergence. Since the solution is independent from the previous time steps, except of course for the penalty term, the alternating minimization algorithm is an implicit solver.

Applied to the energy functional (14), the staggered solver sequentially solves (18a) and (18b) using their respective Jacobian $J^{uu}$ (19a) and $J^{dd}$ (19d) through Newton's method. In this work, we adopt the alternating minimization algorithm as presented in [22, 25] and described in Algorithm 1.

Different stopping criteria are used in the literature, see [28] for a short review. Here, we use a residual-based convergence criteria. Since the two sub-problems are solved sequentially, it is necessary for the inner-Newton methods to be solved to a smaller tolerance to reach the global convergence criteria, implying the necessity of selecting $\texttt{TOL}_N < \texttt{TOL}$ [25].

**Algorithm 1** Alternating minimization scheme

**Input:** $\boldsymbol{U}^{n-1}$, $\boldsymbol{D}^{n-1}$, $\bar{\boldsymbol{U}}^{n}$ on $\Gamma_D$.
**Output:** $\boldsymbol{U}^{n}$, $\boldsymbol{D}^{n}$.

Initialize $\boldsymbol{U}_0 \coloneqq \boldsymbol{U}^{n-1}$, $\boldsymbol{D}_0 \coloneqq \boldsymbol{D}^{n-1}$, $k = 0$.
**while** $||\boldsymbol{R}^d(\boldsymbol{U}_k, \boldsymbol{D}_k)||_{L^\infty} > \texttt{TOL}$ **do**
    Find solution $\boldsymbol{D}_{k+1}$: $\boldsymbol{R}^d(\boldsymbol{U}_k, \boldsymbol{D}_{k+1}) \leq \texttt{TOL}_N$.
    Find solution $\boldsymbol{U}_{k+1}$: $\boldsymbol{R}^u(\boldsymbol{U}_{k+1}, \boldsymbol{D}_{k+1}) \leq \texttt{TOL}_N$.
    $k \leftarrow k + 1$.
**end while**
$\boldsymbol{U}^n \leftarrow \boldsymbol{U}_k$, $\boldsymbol{D}^n \leftarrow \boldsymbol{D}_k$.

*2.2.2. Quasi-monolithic scheme*

Based on the identification of the term $(1-d)^2\sigma^+(\boldsymbol{u}) : e(\boldsymbol{u})$ as the one rendering the functional (14) non-convex, the idea of the quasi-monolithic scheme is to *convexify* the energy functional using a fixed $\tilde{d}$ instead of the unknown field $d$ [13]. $\tilde{d}$ is taken as an extrapolation constructed from the solution of previous time steps, with $\tilde{d} \coloneqq \tilde{d}(d^{n-1}, d^{n-2})$. To obtain a coupled but convex formulation, $\tilde{d}$ is inserted in lieu of $d$ only in equation (16a), rendering the kinematic sub-problem dependant of $\boldsymbol{u}$ only. The damage sub-problem is kept identical to (16b) to preserve the coupling. However, due to the extrapolation $\tilde{d}$, the quasi-monolithic scheme can be interpreted as a semi-implicit method, therefore explaining the numerical viscosity observed in [33].

Different types of extrapolations are used for $\tilde{d}$, such as the linear extrapolation appearing in the implementation published with [13] or the constant extrapolation described in [32]. In fact, many extrapolation schemes could be developed and tested. However, formulation (14) has no dependency in time, implying that no guarantee can be made on the quality of a time-based extrapolation of $d$. By replacing the unknown phase-field with a heuristic prediction as done here, one could reasonably expect the performance of this method to be problem-dependent.

To perform a fair but straightforward comparison between the different methods, we adopt the linear extrapolation, as used in [13, 30, 33] and described in [50] as

$$\tilde{d} = d^{n-1}\frac{t^n - t^{n-2}}{t^{n-1} - t^{n-2}} - d^{n-2}\frac{t^n - t^{n-1}}{t^{n-1} - t^{n-2}}. \tag{21}$$

With the extrapolated scheme, the residual reads

$$\begin{aligned} R_i^u &\coloneqq \int_\Omega \Big((1-\tilde{d}_h)^2\sigma^+(\boldsymbol{u}_h) + \sigma^-(\boldsymbol{u}_h)\Big) : e(\boldsymbol{\phi}_i)\,\mathrm{d}\boldsymbol{x} = 0 \\ R_i^d &\coloneqq \int_\Omega -(1-d_h)\varphi_i\sigma^+(\boldsymbol{u}_h) : e(\boldsymbol{u}_h)\,\mathrm{d}\boldsymbol{x} + \frac{3G_c}{8}\int_\Omega \Big(\frac{\varphi_i}{l} + 2l\nabla d_h \cdot \nabla\varphi_i\Big)\mathrm{d}\boldsymbol{x} \\ &\quad + \gamma\int_\Omega \varphi_i\langle d_h - d_h^{n-1}\rangle_-\,\mathrm{d}\boldsymbol{x} = 0 \end{aligned} \tag{22}$$

with the Jacobian

$$
\begin{aligned}
J_{ij}^{uu} &= \frac{\partial R_i^u}{\partial U_j} = \int_\Omega \Big( (1-\tilde{d}_h)^2 \sigma^+(\boldsymbol{\phi}_j) + \sigma^-(\boldsymbol{\phi}_j) \Big) : e(\boldsymbol{\phi}_i)\,\mathrm{d}\boldsymbol{x} \\
J_{ij}^{ud} &= \frac{\partial R_i^u}{\partial D_j} = 0 \\
J_{ij}^{du} &= \frac{\partial R_i^d}{\partial U_j} = \int_\Omega -2(1-d_h)\varphi_i \sigma^+(\boldsymbol{u}_h) : e(\boldsymbol{\phi}_j)\,\mathrm{d}\boldsymbol{x} \\
J_{ij}^{dd} &= \frac{\partial R_i^d}{\partial D_j} = \int_\Omega \varphi_i \varphi_j \sigma^+(\boldsymbol{u}_h) : e(\boldsymbol{u}_h)\mathrm{d}\boldsymbol{x} + \frac{3G_c}{8}\int_\Omega 2l \nabla\varphi_i \cdot \nabla\varphi_j \mathrm{d}\boldsymbol{x} \\
&\quad + \gamma \int_\Omega \varphi_i \varphi_j H^-(d_h - d_h^{n-1})\,\mathrm{d}\boldsymbol{x}
\end{aligned}
\qquad . \tag{23}
$$

For every time step $t^n$, the solution $\boldsymbol{U} \coloneqq \{\boldsymbol{u}^n, d^n\}$ is obtained with the Newton method using the modified residual $\boldsymbol{R}$ (22) and Jacobian $J$ (23). In this case, the Newton method would consist in solving the linear system

$$
J_k \boldsymbol{\delta U}_k = -\boldsymbol{R}_k \tag{24}
$$

and updating the solution $\boldsymbol{U}_k$ through

$$
\boldsymbol{U}_{k+1} = \boldsymbol{U}_k + \boldsymbol{\delta U}_k \tag{25}
$$

until the convergence criteria is reached. Here, we use the residual based convergence criteria $||\boldsymbol{R}(\boldsymbol{U}_k)||_{L^\infty} \leq$ `TOL`.

## 3. New solution algorithms

### *3.1. A modified Newton method with inertia correction and energy line-search*

When minimizing a function $\mathcal{E}(\boldsymbol{u})$ with Newton's method, a positive definite Hessian, or Jacobian, guarantees the identified search direction $\boldsymbol{\delta u}_k$ to be one of descent. A descent direction implies the existence of a solution $\boldsymbol{u}_{k+1} \coloneqq \boldsymbol{u}_k + \alpha_k \boldsymbol{\delta u}_k$, with the step-size parameter $\alpha_k \in [0,1]$, such that $\mathcal{E}(\boldsymbol{u}_{k+1}) < \mathcal{E}(\boldsymbol{u}_k)$. Therefore, if the Jacobian is positive definite and a line-search procedure is used to identify a satisfying $\alpha_k$, the convergence to a local minimum is theoretically guaranteed [51].

To preserve this convergence property when solving phase-field models, we propose to use a modified Newton method that ensures the positive definiteness of the Jacobian through inertia corrections. The inertia of an $n \times n$ matrix is expressed with the triplet $(a, b, c)$, where $a$, $b$ and $c$ are respectively the number of positive, negative and null eigenvalues, counting the multiplicities. Consequently, the inertia of a positive definite Jacobian of size $n \times n$ should be $(n, 0, 0)$. Since the inertia is available as an output with symmetric indefinite linear solvers such as the ones available in Intel® MKL and HSL, it suffices to verify that $a = n$ before taking a step in the search direction. If the Jacobian is not positive definite, we correct it by adding multiples of the identity matrix, yielding the modified Newton step

$$
(J_k + \delta_k I)\boldsymbol{\delta U}_k = -\boldsymbol{R}_k, \tag{26}
$$

where $\delta_k$ is a scalar parameter and $I$ is the identity matrix. To choose $\delta_k$, we adopt the inertia correction algorithm used in the optimization software IPOPT [37]. The modified Newton method combining system (26) with the inertia correction scheme is presented in Algorithm 2. As can be seen in Algorithm 2, we first attempt to obtain a search direction without corrections. If an incorrect inertia is detected, a first small correction $\bar{\delta}$ is tested. If the correction is still insufficient, the correction is increased by $\kappa^+$ until all eigenvalues are positive. If a correction is needed in a subsequent iteration, the last used value of $\delta$ is reused as a starting point, with a slight decrease by $\kappa^-$. $\bar{\delta}^{min}$ and $\bar{\kappa}^+$ denote the smallest correction accepted and the first increase used in an iteration. The $\kappa^+$, $\kappa^-$, $\bar{\kappa}^+$, $\bar{\delta}$ and $\bar{\delta}^{min}$ parameters appearing in Algorithm 2 are indeed numerical parameters that could be tuned. However, as will be shown in Section 4, significant and

consistent gains in performance are obtained with this method without any tuning and by simply taking the default parameters of IPOPT.

Therefore, for every time step $t^n$, the solution $\boldsymbol{U} \coloneqq \{\boldsymbol{u}^n, d^n\}$ is obtained by identifying a search direction $\boldsymbol{\delta U}_k$ using Algorithm 2, with residual $\boldsymbol{R}_k$ (18) and the full Jacobian (19), and updating the solution $\boldsymbol{U}_k$ with

$$\boldsymbol{U}_{k+1} = \boldsymbol{U}_k + \alpha_k \boldsymbol{\delta U}_k \tag{27}$$

until the convergence criteria is reached. Once again, we use the residual based convergence criteria $||\boldsymbol{R}(\boldsymbol{U}_k)||_{L^\infty} \leq \texttt{TOL}$. $\alpha_k$ is identified through a standard Armijo backtracking line-search applied to the energy functional (14).

The described modified Newton method presents many theoretical and numerical advantages over the phase-field solvers found in the literature. First, since the Jacobian is modified only when necessary, the theoretical quadratic convergence rate of the Newton method is preserved in as many time steps as possible. Once the Jacobian is modified, the convergence rate remains linear [51]. Note also that the corrections appear naturally within the method, and therefore, no switch to a different algorithm is required. Second, instead of relying on the monitoring of some heuristic metric, the method automatically corrects the Jacobian when an incorrect inertia is detected, implying that no *bad* steps are taken before modifying the Jacobian. Finally, as opposed to methods relying only on the residual and Jacobian, the use of a line-search on the energy functional ensures that the solution is at least a local minimum. Altogether, these multiple advantages make the proposed modified Newton method a potentially highly efficient and robust fully monolithic solver for phase-field models.

**Algorithm 2** Modified Newton method with inertia correction

**Input:** $J_k$, $\boldsymbol{R}_k$, $\delta_{k-1}$, $\kappa^+$, $\kappa^-$, $\bar{\kappa}^+$, $\bar{\delta}$, $\bar{\delta}^{min}$.
**Output:** $\boldsymbol{\delta U}_k$, $\delta_k$.

Initialize $\delta^0 = 0$, $i = 0$.
Solve $(J_k + \delta^0 I)\boldsymbol{\delta U}^0 = -\boldsymbol{R}_k$ for $\boldsymbol{\delta U}^0$ and the inertia $(a, b, c)$.
**if** the modified Jacobian is not positive definite, i.e. $a \neq n$ **then**
    **if** $\delta_{k-1} = 0$ **then**
        Set $\delta^1 = \bar{\delta}$
    **else**
        Set $\delta^1 = \max(\bar{\delta}^{min}, \kappa^- \delta_{k-1})$
    **end if**
    Solve $(J_k + \delta^1 I)\boldsymbol{\delta U}^1 = -\boldsymbol{R}_k$ for $\boldsymbol{\delta U}^1$ and the inertia $(a, b, c)$.
    $i \leftarrow i + 1$
    **while** the modified Jacobian is not positive definite, i.e. $a \neq n$ **do**
        **if** $\delta_{k-1} = 0$ **then**
            Set $\delta^{i+1} = \bar{\kappa}^+ \delta^i$
        **else**
            Set $\delta^{i+1} = \kappa^+ \delta^i$
        **end if**
        Solve $(J_k + \delta^{i+1} I)\boldsymbol{\delta U}^{i+1} = -\boldsymbol{R}_k$ for $\boldsymbol{\delta U}^{i+1}$ and the inertia $(a, b, c)$.
        $i \leftarrow i + 1$
    **end while**
**end if**
$\boldsymbol{\delta U}_k \leftarrow \boldsymbol{\delta U}^i$, $\delta_k \leftarrow \delta^i$.

### *3.2. An improved quasi-monolithic scheme using an extrapolation correction loop*

The quasi-monolithic scheme as described in Section 2.2.2 is a semi-implicit method, implying that, depending on the step size, the solution can be delayed or completely inaccurate (see [33] for an example).

The lag in the solution can be explained by the extrapolation $\tilde{d}$ underestimating the rapidly evolving damage field when too large time steps are used. Due to the absence of time-continuity of the damage field, large time steps can cause the extrapolation to quickly diverge from the actual solution.

The simplest strategy to lessen the lag induced by the extrapolation is to use uniformly refined time steps. On one hand, this method usually yields a more accurate solution, since, with the step size converging to zero, the time-based extrapolation can reasonably be expected to converge to the monolithic solution. On the other hand, the uniformly refined time steps imply additional and unnecessary calculations when no crack is propagating. One could consider the use of a time adaptive scheme, but once again, the lack of continuity in time of the damage field hinders the potential robustness of such methods. To the best of our knowledge, no such time adaptive scheme is available for the quasi-monolithic scheme in the literature.

Another strategy to reduce the lag in the evolution of the damage field, as proposed in [50], is to use an additional loop in which the extrapolation is updated. The idea is that, by updating the extrapolation inside a single time step, $\tilde{d}$ should get closer and eventually converge to the actual damage solution $d$.

Rather than using a constant and maybe insufficient number of updates, we propose to continue the iterating process until the damage field reaches a convergence criteria. The solution is defined as converged when the updating of the extrapolation no longer influences the phase-field solution, within a certain tolerance, as

$$||d_k - d_{k-1}||_{L^2} \leq \texttt{TOL}_{\texttt{QM}}. \tag{28}$$

The proposed extrapolation correction loop is heuristic since $d$ has no regularity in time, but it allows the semi-implicit quasi-monolithic scheme to converge to the implicit solution without a uniform time step refinement or constant number of extrapolation correction. The final quasi-monolithic method is detailed in Algorithm 3.

**Algorithm 3** Quasi-monolithic scheme with extrapolation correction loop

**Input:** $\boldsymbol{U}^{n-1}$, $\boldsymbol{D}^{n-1}$, $\boldsymbol{D}^{n-2}$, $\bar{\boldsymbol{U}}^{n}$ on $\Gamma_D$.
**Output:** $\boldsymbol{U}^{n}$, $\boldsymbol{D}^{n}$.

Initialize $\boldsymbol{U}_0 \coloneqq \boldsymbol{U}^{n-1}$, $\boldsymbol{D}_0 \coloneqq \boldsymbol{D}^{n-1}$, $\boldsymbol{D}_{-1} \coloneqq \boldsymbol{D}^{n-2}$, $k = 1$.
Compute extrapolation $\tilde{\boldsymbol{D}}_1 \coloneqq f(\boldsymbol{D}_0, \boldsymbol{D}_{-1})$.
Find solution $\{\boldsymbol{U}_1, \boldsymbol{D}_1\}$: $\boldsymbol{R}(\boldsymbol{U}_1, \boldsymbol{D}_1, \tilde{\boldsymbol{D}}_1) \leq \texttt{TOL}$.
**while** $||\boldsymbol{D}_k - \boldsymbol{D}_{k-1}||_{L^2} > \texttt{TOL}_{\texttt{QM}}$ **do**
    Compute extrapolation $\tilde{\boldsymbol{D}}_{k+1} \coloneqq f(\boldsymbol{D}_k, \boldsymbol{D}_{k-1})$.
    Find solution $\{\boldsymbol{U}_{k+1}, \boldsymbol{D}_{k+1}\}$: $\boldsymbol{R}(\boldsymbol{U}_{k+1}, \boldsymbol{D}_{k+1}, \tilde{\boldsymbol{D}}_{k+1}) \leq \texttt{TOL}$.
    $k \leftarrow k + 1$.
**end while**
$\boldsymbol{U}^n \leftarrow \boldsymbol{U}_k$, $\boldsymbol{D}^n \leftarrow \boldsymbol{D}_k$.

## 4. Numerical results

In this section, we present benchmarks representative of numerical experiments found in the phase-field literature. For all tests and for each algorithm, we compare the resultant crack paths, the force-displacement responses of the structure, the number of iterations required and the computation time. We define an iteration as every time a correction is made to the solution $(\boldsymbol{u}^n, d^n)$. This definition implies that iterations do not have the same associated computational cost depending on the algorithm. Nevertheless, we consider the total number of iterations to inform on the performance of the algorithms when combined with the computation time.

Only 2D geometries are considered and plain strain is assumed. For every geometry, a local mesh refinement with a maximum size of $h = \frac{l}{5}$ is used in the expected fracture zone to avoid a numerical overestimation of the toughness [24, 52, 53]. Pre-existing cracks are modeled as notches in the geometry and mesh. All meshes were generated using the commercial finite element software ABAQUS. The boundary

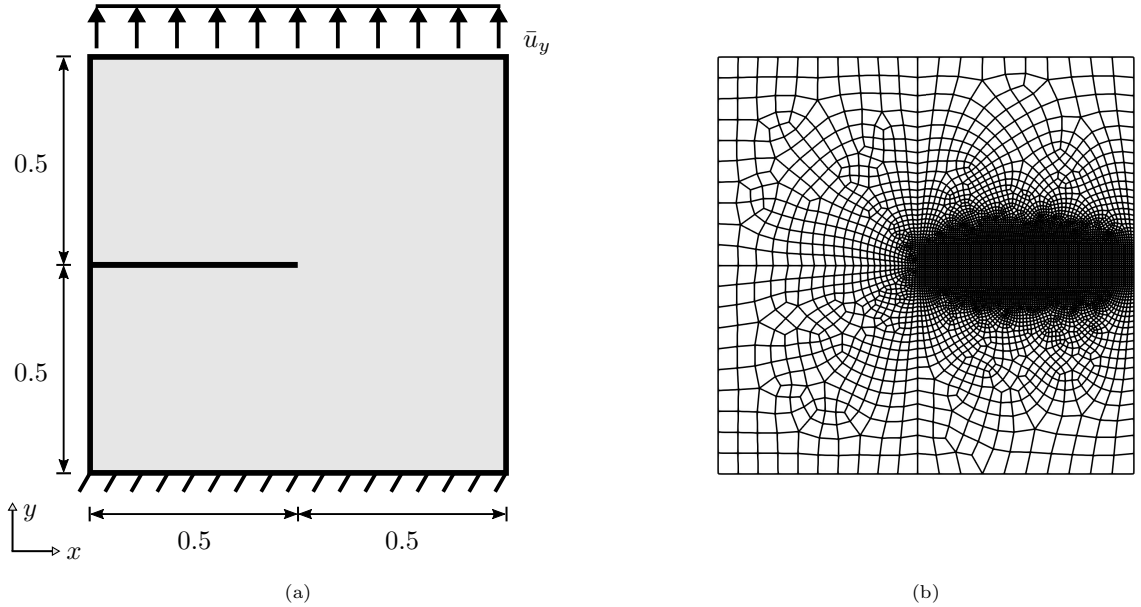


(a) (b)

Figure 1: Single edge notched plate under tension (SENP-tension) test. (a) Schematic of the geometry and boundary conditions. The lower edge of the plate is fixed (i.e. $\bar{u}_x = \bar{u}_y = 0$) while only a vertical displacement of $\bar{u}_y = 0.01$ mm is prescribed on the upper edge. The plate has unit thickness. All units are in mm. (b) Finite element discretization of the geometry.

conditions are strongly enforced by isolating the degrees of freedom subject to the Dirichlet condition and reducing the linear system. Only homogeneous Neumann conditions are considered in this work. The integrals are approximated using the Gauss quadrature with four integration points.

For the penalty coefficient, an irreversibility tolerance of $\texttt{TOL}_{\texttt{Ir}} = 0.01$ is taken as suggested in [25]. For all three methods, the convergence tolerance on the residual is set to $\texttt{TOL} = 10^{-4}$. The tolerance of the inner Newton methods of the alternating algorithm is set to $\texttt{TOL}_N = 10^{-5}$. In order to propose the fairest comparison with the quasi-monolithic scheme, the tolerance $\texttt{TOL}_{QM}$ is adjusted for each experiment to ensure convergence to the implicit solution while minimizing the computation time. For the inertia correction scheme of the modified Newton solver, we take the default IPOPT parameters with $\kappa^+ = 8$, $\kappa^- = \frac{1}{3}$, $\bar{\kappa}^+ = 100$, $\bar{\delta} = 10^{-4}$ and $\bar{\delta}^{min} = 10^{-20}$ [37].

The finite element method and the numerical algorithms presented are implemented using the Julia language [54]. For all three methods, linear systems are solved with the Intel® MKL Pardiso direct sparse solver. All computations are performed on a workstation with an Intel® Core(TM) i7-6700K CPU @ 4.00GHz and 32 GB RAM.

### *4.1. Single-edge notched plate under tensile loading*

As a first test case, we consider the simple notched square plate under uniaxial tension (SENP-tensile). Widely used as a reference test in the literature [10, 35, 36], the geometry and loading generate unstable crack propagation. With an implicit scheme, the crack is expected to fully extend across the plate within a single time increment. Therefore, this test allows to assess the capacity of the algorithms to capture fast propagating cracks.

The geometry, the boundary conditions and the mesh used for this test are presented in Figure 1. The material properties selected are $E = 210$ GPa, $\nu = 0.3$, $G_c = 2.7$ N/mm and $l = 0.024$ mm. A total vertical displacement of 0.01 mm is applied in 50 time steps, implying uniform increments of $\Delta\bar{u} = 2 \times 10^{-4}$. The finite element mesh contains 6524 nodes and 6431 quadrilateral elements. A tolerance of $\texttt{TOL}_{QM} = 0.01$ was found sufficient for the extrapolated scheme to converge to the implicit solution.

Figure 2 shows the crack paths obtained with the three methods for the SENP-tensile tests. As depicted, all three algorithms converge to the expected solution, which in this case is a straight crack from the pre-crack to the right edge. Figure 3 presents the force-displacement response given by the alternating minimization, quasi-monolithic and modified Newton solvers. As can be seen, the three methods are able to capture the instantaneous propagation, with all solutions coinciding and the load dropping to zero in a single time step. It also confirms that the quasi-monolithic scheme coupled with the extrapolation correction loop, as presented in Algorithm 3, converges to the implicit solution.

Figure 4 shows the total number of iterations required for each algorithm to converge with the evolution of the boundary conditions. At time step 31, where the crack is propagating, the modified Newton solver requires only 257 iterations, as opposed to the 406 and 963 needed by the quasi-monolithic scheme and the alternating minimization algorithm, respectively. Table 1 summarizes the number of iterations and the computation time required by the three algorithms for the SENP-tensile test. As can be seen, the decrease in iteration obtained with the modified Newton solver yields a reduction of the computation time by factors of 1.53 and 1.19 compared to the staggered and extrapolated solvers. However, damage propagation is present in only one increment. Consequently, this benchmark does not fully expose the efficiency of the proposed method.

### *4.2. Single-edge notched plate under shear loading*

The notched square plate under shear loading (SENP-shear) is another widely adopted test in the phase-field community since it allows the verification of the energy splitting method [25, 35, 36, 42, 43]. This test is also interesting when studying the efficiency of solvers since it produces a stable crack propagation, the key difficulty when solving phase-field models. From the latter numerical experiments found in the literature, it appears that only [25] reported results for the $AT_1$ model. We used the same parameters in order to allow a comparison with the results from [25], with $E = 210$ GPa, $\nu = 0.3$, $G_c = 2.7$ N/mm and $l = 0.01$ mm. The geometry, the boundary conditions and the mesh are presented in Figure 5. A total horizontal displacement of 0.015 mm is applied in 50 equal increments. The mesh is made of 23341 nodes assembled in 23205 elements. In this case, a smaller tolerance of $\texttt{TOL}_{QM} = 5 \times 10^{-3}$ was required because a delay of the initiation and an oscillation of the reaction force were observed for a greater tolerance (results not shown).

Figure 6 shows the crack paths obtained for the SENP-shear test. As expected and consistently with the results found in the literature (see for example [36]), the cracks initiate from the pre-crack and converge in a curved trajectory towards the lower right corner. The cracks yielded by the three solvers are virtually identical. Figure 7 presents the load-displacement curves obtained with the three solvers for the SENP-shear test. The responses of the three solvers coincide and match with that of [25]. The difference in peak force can be explained by their use of $P_1$ triangular elements and a mesh size of $h = \frac{l}{4}$.

The cumulative number of iterations required by the three solvers is presented in Figure 8. The efficiency of the modified Newton method is clearly illustrated, with a total number of iterations an order of magnitude lower than the quasi-monolithic and alternating schemes. Table 2 summarizes the computational performances of the three methods for the SENP-shear test. As presented, the total number of iterations required by the modified Newton solver is respectively 15 and 7 times lower when compared to the staggered and the extrapolated scheme. On our workstation, the iteration reduction meant a decrease in computation time by factors of respectively 9.25 and 6.40. Finally, one can observe from Figure 8 that the quasi-monolithic scheme is as efficient as the monolithic modified Newton method prior to the damage propagation. However, the efficiency significantly decreases once the crack starts propagating.

### *4.3. Three-point bending test*

Let us now consider the classic three-point bending of a notched beam as presented in [36], which produces a stable mode-I crack propagation. The geometry, the loading and the discretization used are depicted in Figure 9. We adopt the same material properties as in [36], with $E = 20.8$ GPa, $\nu = 0.3$ and $G_c = 0.54$ N/mm. It should be noted, however, that simulations performed in [36] were made using the $AT_2$ model. In order to have equivalent mechanical properties for the $AT_1$ model, the characteristic length is converted using the solution for a homogeneous bar under uniaxial tension [24]. The conversion yields a characteristic


(a) Alternating minimization (b) Quasi-monolithic (c) Modified Newton

Figure 2: Comparison of the final crack patterns ($\bar{u}_y = 0.01$ mm) for the three studied algorithms on the undeformed geometry of the SENP-tension test. Crack paths obtained with the three methods are in agreement. The crack produced by the quasi-monolithic (b) scheme has initiated from below the notch, as opposed to the two other methods where the crack initiated above the notch. The difference remains however negligible.

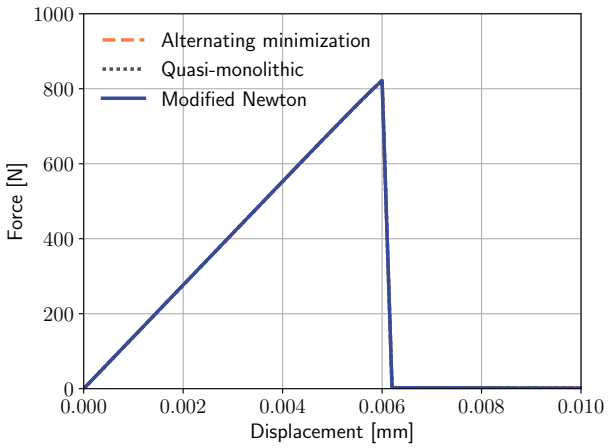


Figure 3: Load-displacement curves obtained with the different solvers on the SENP-tension test. The three algorithms produce identical solutions.

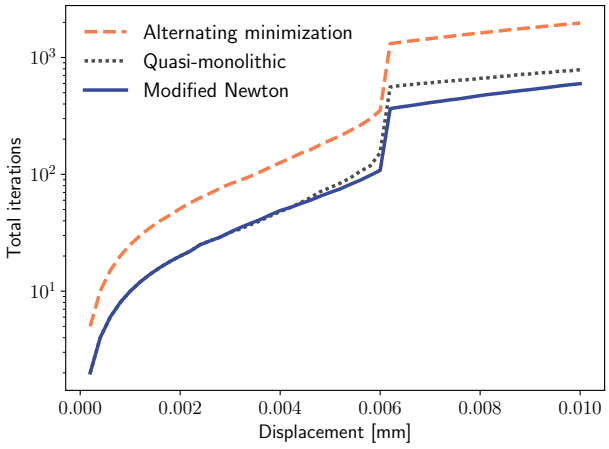


Figure 4: Total number of iterations required for the different algorithms to converge on the SENP-tension test. The modified Newton solver appears as the most efficient, while the extrapolated scheme also shows a reduction of the number of iterations when compared to the alternating minimization algorithm.

Table 1: Comparison of the iterations and computation time required for the studied algorithms to solve the SENP-tension benchmark.

| Method | Total it. | Max it. / inc. | Time (s) |
|---|---|---|---|
| Alternating minimization | 1972 | 963 | 514 |
| Quasi-monolithic | 787 | 406 | 400 |
| Modified Newton | 597 | 257 | 336 |

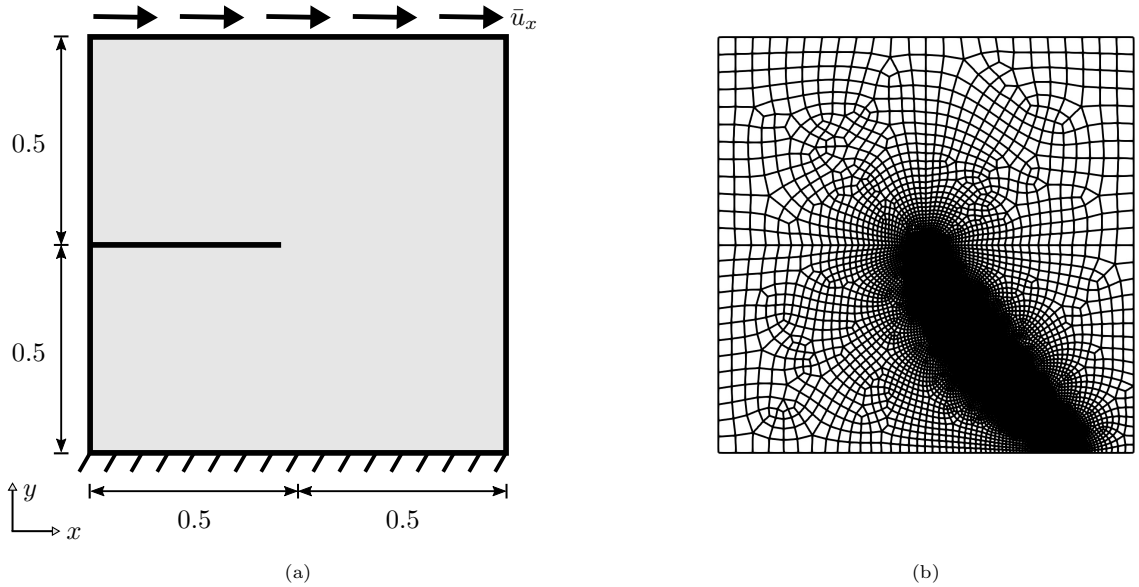


(a) (b)

Figure 5: Single edge notched plate under shear (SENP-shear) test. (a) Illustration of the geometry and boundary conditions. The lower edge of the plate is fixed (i.e. $\bar{u}_x = \bar{u}_y = 0$). An horizontal displacement of $\bar{u}_x = 0.015$ mm is prescribed on the upper edge while maintaining $\bar{u}_y = 0$. The plate has a unit thickness. The units are in mm. (b) Finite element discretization.

length of $l = 0.101$ mm. A total displacement of 0.1 mm discretized in 50 equal increments is applied as illustrated in Figure 9. 11181 nodes and 11031 elements are used. As in the SENP-tension test, a tolerance of $\texttt{TOL}_{QM} = 0.01$ was found sufficient for the quasi-monolithic scheme to converge to the implicit solution.

The resulting crack patterns for the three-point bending test are shown in Figure 10. As expected for a mode-I fracture, the cracks for all three solvers propagate from the notch to the upper edge in a straight line. Once again, they are virtually identical with only a negligible offset for the solution obtained through the modified Newton solver. Figure 11 presents the load-deflection curves obtained for the three-point bending test with the three methods. The solutions are identical and in good agreement with that reported in [36].

Figure 12 presents the cumulative iterations required by the three solvers to obtain a solution to the phase-field problem. As illustrated, the quasi-monolithic and the modified-Newton methods have a similar efficiency before the propagation of damage. However, once the crack starts propagating, the modified Newton algorithm clearly outperforms the alternating and quasi-monolithic schemes. Table 3 shows the total iterations, maximum iterations in an increment and calculation time required by the three algorithms. The modified Newton solver requires a maximum of only 193 iterations, compared to the 565 and 989 of the extrapolated and alternating scheme respectively. This is a reduction in iterations by factors of $\approx 3$ and $\approx 5$, which translates to an acceleration of the computation by factors of 3.33 and 4.18, respectively.

### *4.4. L-shaped panel test*

The concrete L-shaped panel with mixed mode crack propagation from [55] is another popular experiment used to evaluate and validate phase-field models [28, 32, 33, 36, 53]. We adopt the geometry, loading and material properties from [53] for comparison purposes. The geometry, boundary conditions and mesh are presented in Figure 13. The material parameters are $E = 21.85$ GPa, $\nu = 0.18$, $G_c = 0.095$ N/mm and $l = 3.125$ mm. A total vertical displacement of 1.0 mm is applied as described in Figure 13. 50 equal increments are used to discretize the loading process. The finite element mesh is made of 48984 nodes and 48850 quadrilateral elements. A tolerance of $\texttt{TOL}_{QM} = 5 \times 10^{-3}$ is used for the results presented for the quasi-monolithic scheme, but as will be shown in the following, no convergence to the implicit solution was obtained.


(a) Alternating minimization (b) Quasi-monolithic (c) Modified Newton

Figure 6: Comparison of the final crack paths at $\bar{u}_x = 0.015$ mm for all three studied methods on the undeformed geometry of the SENP-shear test. All three crack patterns are virtually identical.

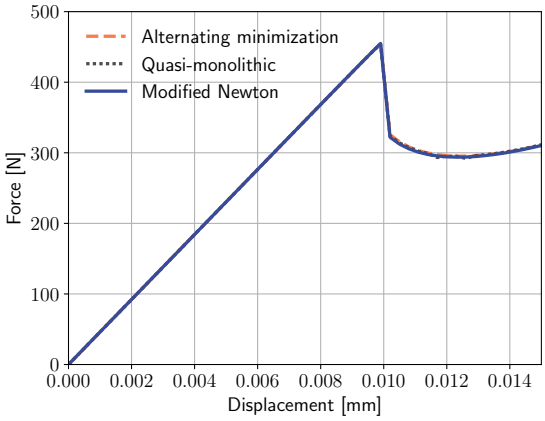


Figure 7: Load versus displacement obtained with the three solvers for the SENP-shear test. The three solutions coincide.

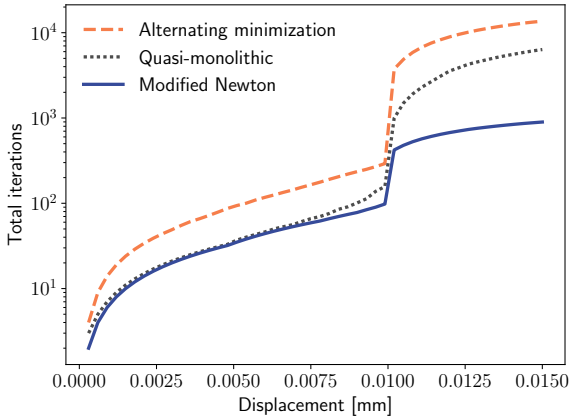


Figure 8: Cumulative number of iterations required by the algorithms depending on the applied displacement in the SENP-shear test. The modified Newton solver clearly necessitates less iterations when the damage starts propagating.

Table 2: Comparison of the computational performances of the three algorithms on the SENP-shear test.

| Method | Total it. | Max it. / inc. | Time (s) |
|---|---|---|---|
| Alternating minimization | 13654 | 3454 | 14403 |
| Quasi-monolithic | 6349 | 838 | 9961 |
| Modified Newton | 897 | 324 | 1557 |

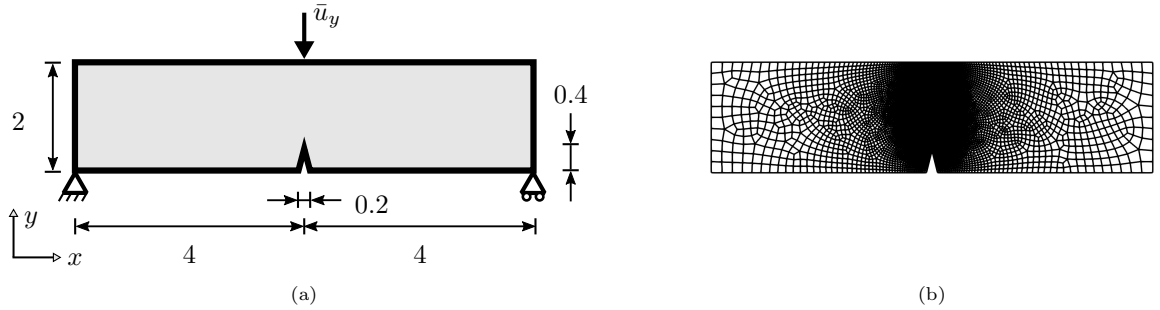


Figure 9: Three-point bending of a notched beam test. (a) Schematic of the geometry and boundary conditions. The lower left node is fixed (i.e. $\bar{u}_x = \bar{u}_y = 0$), as where the lower right node is only supported vertically and free in $x$ (i.e. $\bar{u}_y = 0$). A vertical displacement of $\bar{u}_y = 0.1$ mm is prescribed on the center node of the upper edge. The beam has a unit thickness. All units are in mm. (b) Finite element discretization of the geometry.

The crack paths obtained with the three solvers for the L-shaped panel tests are shown in Figure 14. The crack patterns resulting from the alternating minimization and the IPOPT solvers are identical and in agreement with results found in the literature, e.g. [33, 36, 53], where the crack first propagate with an angle and stabilizes in the horizontal direction. A small deviation is observed at the end of the crack path but the results still concur with experimentally observed fractures [55]. Figure 15 shows the load-displacement curves obtained for the L-shaped panel with the three algorithms. Again here, the alternating minimization and IPOPT solvers are in agreement. The response also concurs with the results obtained without the research for a global minimum in [53]. The difference in peak load can be explained by the absence of a tension/compression split and the crack initiation performed in [53].

The crack and the load-displacement curve obtained with the quasi-monolithic scheme are in agreement with neither the numerical results obtained from the two other methods nor the experimental results reported in [55]. Furthermore, the obtained crack path is physically questionable since it does not agree with the principle of local symmetry, stating that the crack should propagate in a direction allowing the crack tip to be purely in mode-I [56]. This error can be attributed to the extrapolation correction loop, which in the present case appears to have significantly influenced the solution. However, either no convergence to the implicit solution or no convergence to a stationary point was obtained with different tolerances $\texttt{TOL}_{QM}$ or different uniform time refinements.

Figure 16 presents the performance of the three algorithms for the L-shaped panel test, although the results for the extrapolated scheme should be interpreted carefully since the method did not converge to the same solution. As can be seen, the final total iterations required by the IPOPT solver is lower than the alternating minimization algorithm by approximately an order of magnitude. Table 4 summarizes the performances of the three methods for the L-shaped panel test. As noted in Table 4, a staggering number of iterations was required by the alternating minimization algorithm to solve increment 14 ($\bar{u}_y = 0.28$). In comparison, the IPOPT solver required 10.60 times less iterations for the same increment. Nevertheless, the 6455 iterations of the IPOPT solver for this time step remains large. The high computational cost associated to increment 14 can be explained by the sudden propagation of a large crack and possibly ill-conditioned systems. However, the conditioning of the systems was not further investigated. Regardless, an overall acceleration of the computation time by a factor of $\approx 6.5$ was still observed with the proposed method and the efficiency gain obtained with the IPOPT solver is consistent with the results of the previous tests.

### *4.5. Discussion of the results*

We recall that the alternating minimization algorithm, the quasi-monolithic scheme and the method relying on the IPOPT software all used the same numerical implementation and treatment of the irreversibility condition. The difference remained in the algorithm used to obtain a stationary point or local minimum. The benchmarking on the four tests, selected from the phase-field literature, showed that both the extrap-

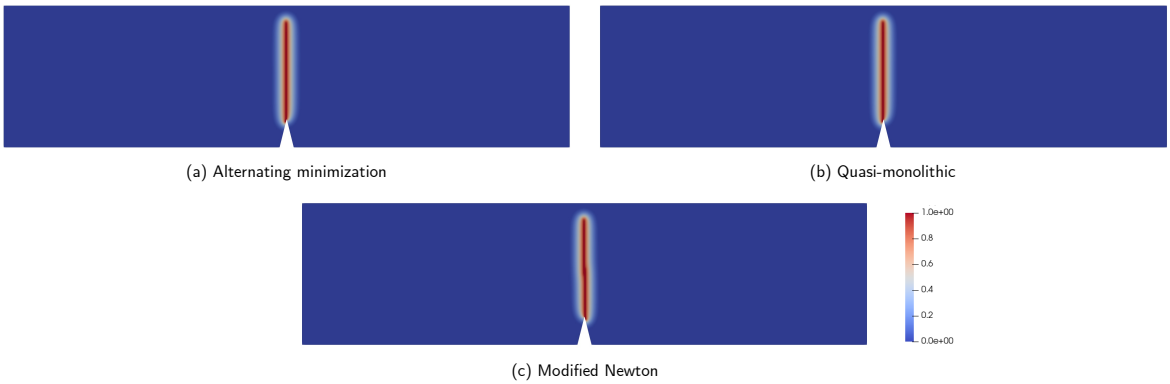


Figure 10: Final crack paths for the three methods on the notched beam under three-point bending for a total deflection of $\bar{u}_y = 0.1$ mm. The three cracks are closely similar, however, the crack produced by the modified Newton solver (c) initiated from the right-hand side of the notch, as opposed to the alternating minimization (a) and quasi-monolithic (b) schemes where the crack initiated to the left-hand side.

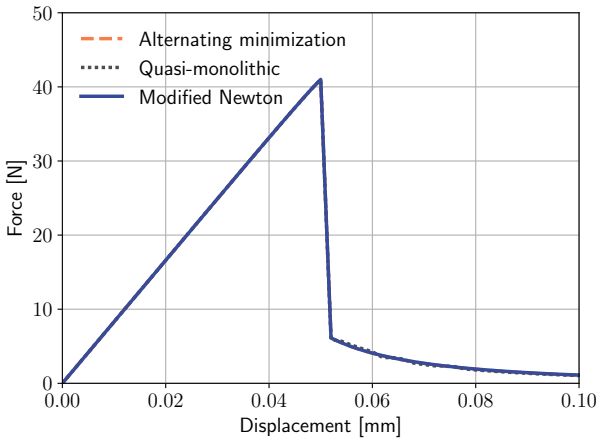


Figure 11: Load-deflection curve of the three-point bending experiment for the different algorithms. Again, all three solutions coincide.

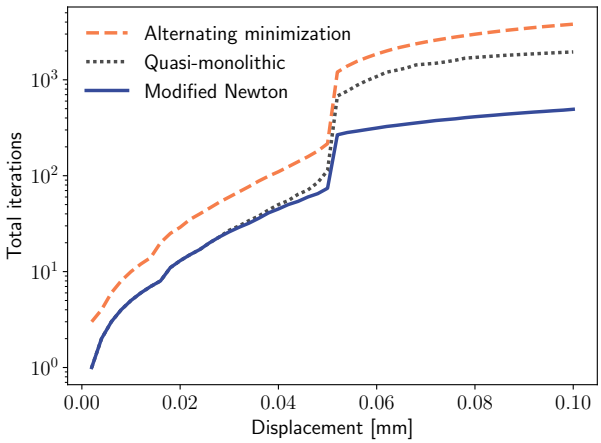


Figure 12: Total number of iterations required by the methods depending on the deflection of the notched beam. Before the crack propagation, the quasi-monolithic scheme is as efficient as the modified Newton method. Once the crack starts propagating, the modified Newton method is clearly the most efficient solver.

Table 3: Computational performances of the different studied methods on the three-point bending test.

| Method | Total it. | Max it. / inc. | Time (s) |
|---|---|---|---|
| Alternating minimization | 3804 | 989 | 1969 |
| Quasi-monolithic | 1953 | 565 | 1567 |
| Modified Newton | 493 | 193 | 471 |

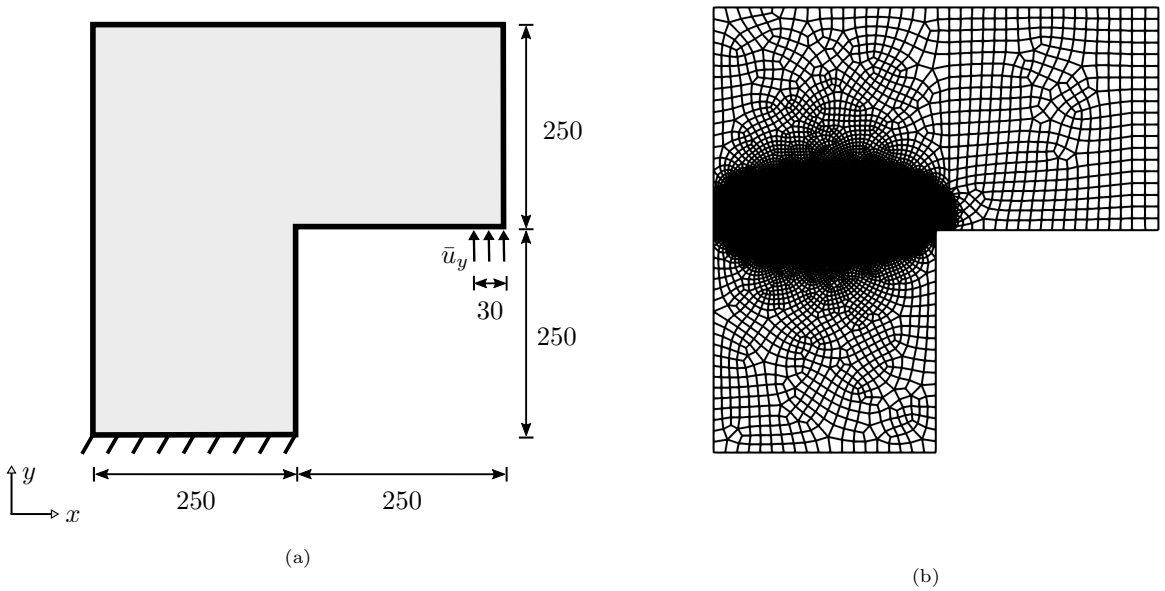


(a) (b)

Figure 13: L-shaped panel test. (a) Respresentation of the geometry and boundary conditions. The lower edge is fixed (i.e. $\bar{u}_x = \bar{u}_y = 0$) and a vertical displacement of $\bar{u}_y = 1.0$ mm is prescribed as indicated on the figure. The panel has a thickness of 100 mm. The units are in mm. (b) Finite element discretization of the geometry.

olated scheme and the IPOPT method offered an increase in computational efficiency, when compared to the staggered algorithm. However, once damage started propagating, the semi-implicit extrapolated scheme required additional correction to converge to the implicit solution. Consequently, IPOPT was found to be, by far, the most efficient solver. For example on the SENP-shear test, the IPOPT solver required up to 12 and 4 times less iterations by increment than the alternating minimization and quasi-monolithic algorithms, respectively. Similarly, on the same test, diminutions of the total iterations by factors of up to 14 and 6 times were obtained.

The alternating minimization algorithm remains a powerful and versatile method since it can be applied to non-variational models and implemented using a variational inequality solver, like reported in [22, 24]. As for the extrapolated scheme, its performance can probably be enhanced with locally refined time steps and a well-tuned extrapolation. It can also be applied to non-variational formulation. However, convergence problems were encountered with the quasi-monolithic scheme, as observable for the L-shaped panel test. It is possible that the preconditioned GMRES solver reported in [34] would improve the method. Nevertheless, if a variational formulation is available, the results of the four tests clearly exhibit that the IPOPT solver significantly outperforms the alternating minimization and the quasi-monolithic algorithms for quasi-static brittle fracture.

Finally, as already mentioned, convergence issues were sporadically observed with the quasi-monolithic scheme and a surprisingly high number of iterations were necessary for the three methods on the L-shaped panel test. The latter issues are symptomatic of ill-conditioned non-linear systems and could be attributed to the quadratic penalty term used to enforce the irreversibility condition, even if the optimal penalty parameter from [25] was used. As presented in Section 2.1.2, other methods of enforcing the irreversibility condition are available in the literature. Now that an implicit and monolithic solver has been identified, the benchmarking of the schemes used to enforce the $\dot{d} \geq 0$ constraint could allow the identification of a method reducing the issues associated to bad conditioning and minimizing the computational cost associated to the solution of phase-field models.


(a) Alternating minimization (b) Quasi-monolithic (c) IPOPT

Figure 14: Crack paths obtained for the three algorithms after applying a total vertical displacement of $\bar{u}_y = 1.0$ mm. The cracks obtained with the alternating algorithm (a) and IPOPT (c) are identical. The solution produced by the extrapolated scheme (b) appears to be incorrect. The undeformed geometry is shown.

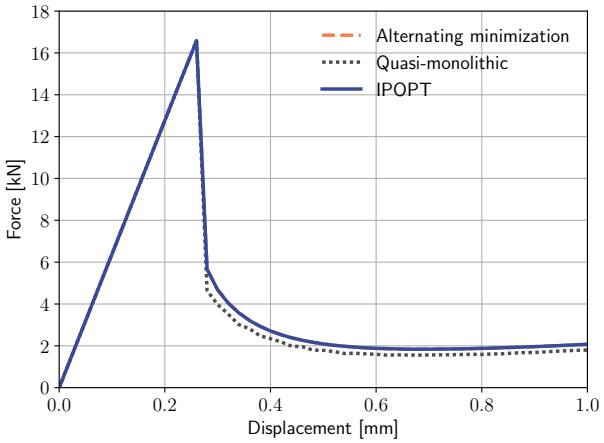


Figure 15: Load-displacement curves resulting from all three methods on the L-shaped panel test. The reaction obtained with the staggered and IPOPT solvers are identical. The response obtained with the quasi-monolithic scheme does not agree with the solutions from the two other methods.

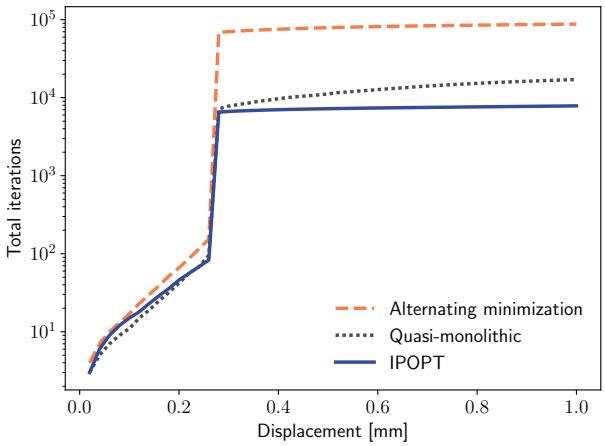


Figure 16: Cumulative number of iterations required by the different methods to solve the L-shaped panel test. IPOPT requires about 10 times less iterations than the alternating method. The curve reported for the quasi-monolithic scheme should be interpreted carefully since the method did not converge to the same solution as the other two methods.

Table 4: Computational performances of the methods investigated on the L-shaped panel benchmark.

| Method | Total it. | Max it. / inc. | Time (s) |
|---|---|---|---|
| Alternating minimization | 87706 | 68442 | 198377 |
| Quasi-monolithic | 17117 | 7093 | 62697 |
| IPOPT | 7855 | 6455 | 31153 |

## 5. Conclusion

A robust, efficient and straightforward solver is still lacking the variational phase-field fracture literature. In an attempt to fill this gap, we proposed a fully monolithic solver using the well-known optimization software IPOPT. Furthermore, the quasi-monolithic algorithm was augmented with an extrapolation correction loop controlled by a damage-based criterion. Although not perfect, the modified quasi-monolithic scheme allowed us to compare its performance with the alternating algorithm and the IPOPT solver. Through the four test cases presented involving different modes of propagation and initiation, we showed the IPOPT solver to be robust and more efficient than the alternating minimization algorithm and the quasi-monolithic scheme. More precisely, the proposed monolithic solver was shown to be up to $\approx 9$ and $\approx 6$ time faster than the staggered and extrapolated schemes. Additionally, the performance of the monolithic method did not appear to be problem-dependent, requiring no parameter adjustment and showing consistent efficiency gains across the test cases.

Additional work can still be done to enhance the performance of phase-field solvers. A lighter implementation of the modified Newton method specific to phase-field models could be developed to replace the general-purpose IPOPT software. As suggested in the discussion, the benchmarking of the methods used to enforce the irreversibility condition could also help further reduce the computational cost of the phase-field method. However, the combination of the IPOPT solver with a mesh adaptation technique could already facilitate the application of phase-field models to more complex structure and with sophisticated constitutive laws.

## Acknowledgements

We thank the Natural Sciences and Engineering Research Council of Canada (NSERC) and the Fonds de recherche du Québec - Nature et technologies (FRQNT) for their support.

## References

[1] A. A. Griffith, The Phenomena of Rupture and Flow in Solids, Philosophical Transactions of the Royal Society A: Mathematical, Physical and Engineering Sciences 221 (582-593) (1921) 163–198. doi:10.1098/rsta.1921.0006.

[2] G. Francfort, J.-J. Marigo, Revisiting brittle fracture as an energy minimization problem, Journal of the Mechanics and Physics of Solids 46 (8) (1998) 1319–1342. doi:10.1016/S0022-5096(98)00034-9.

[3] B. Bourdin, G. Francfort, J.-J. Marigo, Numerical experiments in revisited brittle fracture, Journal of the Mechanics and Physics of Solids 48 (4) (2000) 797–826. doi:10.1016/S0022-5096(99)00028-9.

[4] J.-Y. Wu, V. P. Nguyen, C. T. Nguyen, D. Sutula, S. Sinaie, S. Bordas, Phase-field modeling of fracture, in: Advances in Applied Mechanics, Elsevier, 2019, p. S0065215619300134. doi:10.1016/bs.aams.2019.08.001.

[5] A. Mikelić, M. F. Wheeler, T. Wick, Phase-field modeling of a fluid-driven fracture in a poroelastic medium, Comput Geosci 19 (6) (2015) 1171–1195. doi:10.1007/s10596-015-9532-5.

[6] Z. A. Wilson, C. M. Landis, Phase-field modeling of hydraulic fracture, Journal of the Mechanics and Physics of Solids 96 (2016) 264–290. doi:10.1016/j.jmps.2016.07.019.

[7] C. Miehe, F. Aldakheel, A. Raina, Phase field modeling of ductile fracture at finite strains: A variational gradient-extended plasticity-damage theory, International Journal of Plasticity 84 (2016) 1–32. doi:10.1016/j.ijplas.2016.04.011.

[8] M. J. Borden, T. J. Hughes, C. M. Landis, A. Anvari, I. J. Lee, A phase-field formulation for fracture in ductile materials: Finite deformation balance law derivation, plastic degradation, and stress triaxiality effects, Computer Methods in Applied Mechanics and Engineering 312 (2016) 130–166. doi:10.1016/j.cma.2016.09.005.

[9] T.-T. Nguyen, J. Bolivar, J. Réthoré, M.-C. Baietto, M. Fregonese, A phase field method for modeling stress corrosion crack propagation in a nickel base alloy, International Journal of Solids and Structures 112 (2017) 65–82. doi:10.1016/j.ijsolstr.2017.02.019.

[10] E. Martínez-Pañeda, A. Golahmar, C. F. Niordson, A phase field formulation for hydrogen assisted cracking, Computer Methods in Applied Mechanics and Engineering 342 (2018) 742–761. doi:10.1016/j.cma.2018.07.021.

[11] A. C. Hansen-Dörr, R. de Borst, P. Hennig, M. Kästner, Phase-field modelling of interface failure in brittle materials, Computer Methods in Applied Mechanics and Engineering 346 (2019) 25–42. doi:10.1016/j.cma.2018.11.020.

[12] T.-T. Nguyen, J. Yvonnet, D. Waldmann, Q.-C. He, Phase field modeling of interfacial damage in heterogeneous media with stiff and soft interphases, Engineering Fracture Mechanics 218 (2019) 106574. doi:10.1016/j.engfracmech.2019.106574.

[13] T. Heister, M. F. Wheeler, T. Wick, A primal-dual active set method and predictor-corrector mesh adaptivity for computing fracture propagation using a phase-field approach, Computer Methods in Applied Mechanics and Engineering 290 (2015) 466–495. doi:10.1016/j.cma.2015.03.009.

[14] N. Ferro, S. Micheletti, S. Perotto, Anisotropic mesh adaptation for crack propagation induced by a thermal shock in 2D, Computer Methods in Applied Mechanics and Engineering 331 (2018) 138–158. doi:10.1016/j.cma.2017.11.024.

[15] K. Mang, M. Walloth, T. Wick, W. Wollner, Mesh adaptivity for quasi-static phase-field fractures based on a residual-type a posteriori error estimator, GAMM-Mitteilungen 43 (1). doi:10.1002/gamm.202000003.

[16] R. Patil, B. Mishra, I. Singh, An adaptive multiscale phase field method for brittle fracture, Computer Methods in Applied Mechanics and Engineering 329 (2018) 254–288. doi:10.1016/j.cma.2017.09.021.

[17] L. H. Nguyen, D. Schillinger, The multiscale finite element method for nonlinear continuum localization problems at full fine-scale fidelity, illustrated through phase-field fracture and plasticity, Journal of Computational Physics 396 (2019) 129–160. doi:10.1016/j.jcp.2019.06.058.

[18] H. Amor, J.-J. Marigo, C. Maurini, Regularized formulation of the variational brittle fracture with unilateral contact: Numerical experiments, Journal of the Mechanics and Physics of Solids 57 (8) (2009) 1209–1229. doi:10.1016/j.jmps.2009.04.011.

[19] M. J. Borden, C. V. Verhoosel, M. A. Scott, T. J. Hughes, C. M. Landis, A phase-field description of dynamic brittle fracture, Computer Methods in Applied Mechanics and Engineering 217-220 (2012) 77–95. doi:10.1016/j.cma.2012.01.008.

[20] M. Ambati, T. Gerasimov, L. De Lorenzis, Phase-field modeling of ductile fracture, Comput Mech 55 (5) (2015) 1017–1040. doi:10.1007/s00466-015-1151-4.

[21] T. Nguyen, J. Yvonnet, Q.-Z. Zhu, M. Bornert, C. Chateau, A phase-field method for computational modeling of interfacial damage interacting with crack propagation in realistic microstructures obtained by microtomography, Computer Methods in Applied Mechanics and Engineering 312 (2016) 567–595. doi:10.1016/j.cma.2015.10.007.

[22] J.-J. Marigo, C. Maurini, K. Pham, An overview of the modelling of fracture by gradient damage models, Meccanica 51 (12) (2016) 3107–3128. doi:10.1007/s11012-016-0538-4.

[23] K. H. Pham, K. Ravi-Chandar, C. M. Landis, Experimental validation of a phase-field model for fracture, Int J Fract 205 (1) (2017) 83–101. doi:10.1007/s10704-017-0185-3.

[24] E. Tanné, T. Li, B. Bourdin, J.-J. Marigo, C. Maurini, Crack nucleation in variational phase-field models of brittle fracture, Journal of the Mechanics and Physics of Solids 110 (2018) 80–99. doi:10.1016/j.jmps.2017.09.006.

[25] T. Gerasimov, L. De Lorenzis, On penalization in variational phase-field models of brittle fracture, Computer Methods in Applied Mechanics and Engineering 354 (2019) 990–1026. doi:10.1016/j.cma.2019.05.038.

[26] T. Gerasimov, L. De Lorenzis, A line search assisted monolithic approach for phase-field computing of brittle fracture, Computer Methods in Applied Mechanics and Engineering 312 (2016) 276–303. doi:10.1016/j.cma.2015.12.017.

[27] P. Farrell, C. Maurini, Linear and nonlinear solvers for variational phase-field models of brittle fracture: NUMERICAL SOLUTION OF A VARIATIONAL FRACTURE MODEL, Int. J. Numer. Meth. Engng 109 (5) (2017) 648–667. doi:10.1002/nme.5300.

[28] J.-Y. Wu, Y. Huang, V. P. Nguyen, On the BFGS monolithic algorithm for the unified phase field damage theory, Computer Methods in Applied Mechanics and Engineering 360 (2020) 112704. doi:10.1016/j.cma.2019.112704.

[29] Y. Lu, T. Helfer, B. Bary, O. Fandeur, An efficient and robust staggered algorithm applied to the quasi-static description of brittle fracture by a phase-field approach, Computer Methods in Applied Mechanics and Engineering 370 (2020) 113218. doi:10.1016/j.cma.2020.113218.

[30] S. Lee, A. Mikelić, M. F. Wheeler, T. Wick, Phase-Field Modeling of Two Phase Fluid Filled Fractures in a Poroelastic Medium, Multiscale Model. Simul. 16 (4) (2018) 1542–1580. doi:10.1137/17M1145239.

[31] D. Jodlbauer, U. Langer, T. Wick, Matrix-free multigrid solvers for phase-field fracture problems, arXiv:1902.08112 [math]ArXiv: 1902.08112.

[32] K. Mang, T. Wick, W. Wollner, A phase-field model for fractures in nearly incompressible solids, Comput Mech 65 (1) (2020) 61–78. doi:10.1007/s00466-019-01752-w.

[33] T. Wick, An Error-Oriented Newton/Inexact Augmented Lagrangian Approach for Fully Monolithic Phase-Field Fracture Propagation, SIAM J. Sci. Comput. 39 (4) (2017) B589–B617. doi:10.1137/16M1063873.

[34] T. Wick, Modified Newton methods for solving fully monolithic phase-field quasi-static brittle fracture propagation, Computer Methods in Applied Mechanics and Engineering 325 (2017) 577–611. doi:10.1016/j.cma.2017.07.026.

[35] C. Miehe, M. Hofacker, F. Welschinger, A phase field model for rate-independent crack propagation: Robust algorithmic implementation based on operator splits, Computer Methods in Applied Mechanics and Engineering 199 (45-48) (2010) 2765–2778. doi:10.1016/j.cma.2010.04.011.

[36] M. Ambati, T. Gerasimov, L. De Lorenzis, A review on phase-field models of brittle fracture and a new fast hybrid formulation, Comput Mech 55 (2) (2015) 383–405. doi:10.1007/s00466-014-1109-y.

[37] A. Wächter, L. T. Biegler, On the implementation of an interior-point filter line-search algorithm for large-scale nonlinear programming, Math. Program. 106 (1) (2006) 25–57. doi:10.1007/s10107-004-0559-y.

[38] L. Ambrosio, V. M. Tortorelli, Approximation of functional depending on jumps by elliptic functional via t-convergence, Comm. Pure Appl. Math. 43 (8) (1990) 999–1036. doi:10.1002/cpa.3160430805.

[39] K. Pham, H. Amor, J.-J. Marigo, C. Maurini, Gradient Damage Models and Their Use to Approximate Brittle Fracture, International Journal of Damage Mechanics 20 (4) (2011) 618–652. doi:10.1177/1056789510386852.

[40] G. Lancioni, G. Royer-Carfagni, The Variational Approach to Fracture Mechanics. A Practical Application to the French Panthéon in Paris, J Elasticity 95 (1-2) (2009) 1–30. doi:10.1007/s10659-009-9189-1.

[41] J.-Y. Wu, V. P. Nguyen, A length scale insensitive phase-field damage model for brittle fracture, Journal of the Mechanics and Physics of Solids 119 (2018) 20–42. doi:10.1016/j.jmps.2018.06.006.

[42] C. Bilgen, K. Weinberg, On the crack-driving force of phase-field models in linearized and finite elasticity, Computer Methods in Applied Mechanics and Engineering 353 (2019) 348–372. doi:10.1016/j.cma.2019.05.009.

[43] N. v. Dijk, J. Espadas-Escalante, P. Isaksson, Strain energy density decompositions in phase-field fracture theories for orthotropy and anisotropy, International Journal of Solids and Structures 196-197 (2020) 140–153. doi:10.1016/j.ijsolstr.2020.04.022.

[44] A. Schlüter, A. Willenbücher, C. Kuhn, R. Müller, Phase field approximation of dynamic brittle fracture, Comput Mech 54 (5) (2014) 1141–1161. doi:10.1007/s00466-014-1045-x.

[45] T. Wu, A. Carpiuc-Prisacari, M. Poncelet, L. De Lorenzis, Phase-field simulation of interactive mixed-mode fracture tests on cement mortar with full-field displacement boundary conditions, Engineering Fracture Mechanics 182 (2017) 658–688. doi:10.1016/j.engfracmech.2017.06.014.

[46] C. Kuhn, A. Schlüter, R. Müller, On degradation functions in phase field fracture models, Computational Materials Science 108 (2015) 374–384. doi:10.1016/j.commatsci.2015.05.034.

[47] M. Wheeler, T. Wick, W. Wollner, An augmented-Lagrangian method for the phase-field approach for pressurized fractures, Computer Methods in Applied Mechanics and Engineering 271 (2014) 69–85. doi:10.1016/j.cma.2013.12.005.

[48] S. C. Brenner, L. R. Scott, The Mathematical Theory of Finite Element Methods, Vol. 15 of Texts in Applied Mathematics, Springer New York, New York, NY, 2008. doi:10.1007/978-0-387-75934-0.

[49] W. Bangerth, Assembling matrices in deal.II, Technical report, ETH Zürich (2002).

[50] K. Mang, T. Wick, Numerical Methods for Variational Phase-Field Fracture ProblemsPublisher: Hannover : Institutionelles Repositorium der Leibniz Universität Hannover. doi:10.15488/5129.

[51] J. Nocedal, S. J. Wright, Numerical Optimization, Springer Series in Operations Research and Financial Engineering, Springer New York, 2006. doi:10.1007/978-0-387-40065-5.

[52] B. Bourdin, G. A. Francfort, J.-J. Marigo, The Variational Approach to Fracture, J Elasticity 91 (1-3) (2008) 5–148. doi:10.1007/s10659-007-9107-3.

[53] A. Mesgarnejad, B. Bourdin, M. Khonsari, Validation simulations for the variational approach to fracture, Computer Methods in Applied Mechanics and Engineering 290 (2015) 420–437. doi:10.1016/j.cma.2014.10.052.

[54] J. Bezanson, A. Edelman, S. Karpinski, V. B. Shah, Julia: A Fresh Approach to Numerical Computing, SIAM Rev. 59 (1) (2017) 65–98. doi:10.1137/141000671.

[55] B. J. Winkler, Traglastuntersuchungen von unbewehrten und bewehrten Betonstrukturen auf der Grundlage eines objektiven Werkstoffgesetzes für Beton (PhD thesis), Innsbruck University Press, 2001.

[56] R. V. Gol'dstein, R. L. Salganik, Brittle fracture of solids with arbitrary cracks, Int J Fract 10 (4) (1974) 507–523. doi:10.1007/BF00155254.